

Multimode interferometry for entangling atoms in quantum networks

Thomas D. Barrett,¹ Allison Rubenok,² Dustin Stuart,¹ Oliver Barter,¹ Annemarie Holleccek,^{1,*} Jerome Dilley,¹ Peter B.R. Nisbet-Jones,¹ Konstantinos Poullos,^{2,†} Graham D. Marshall,² Jeremy L. O’Brien,² Alberto Politi,^{2,‡} Jonathan C.F. Matthews,² and Axel Kuhn^{1,§}

¹University of Oxford, Clarendon Laboratory, Parks Road, Oxford OX1 3PU, UK

²Quantum Engineering Technology Labs, H. H. Wills Physics Laboratory and Department of Electrical and Electronic Engineering, University of Bristol, BS8 1FD, UK

(Dated: August 10, 2019)

We operate a multimode interferometer (MMI) integrated onto a photonic chip using pairs of narrowband photons produced from an *a priori* non-probabilistic source. A single ⁸⁷Rb atom strongly coupled to a high-finesse optical cavity provides the light-matter interface that realises the highly controllable emission of single-photons. Non-classical correlations between photon detection events show no loss of coherence when interfering pairs of these photons through the MMI in comparison to the two-photon visibility directly measured using Hong-Ou-Mandel interference on a beam splitter. This demonstrates the ability of integrated multimode circuits to mediate the entanglement of remote nodes in a quantum network interlinked by photonic qubits.

I. INTRODUCTION

Entanglement is an essential resource for many applications of quantum information processing (QIP). In particular the creation of entanglement between remote nodes of distributed quantum networks is a key goal of the field [1–3]. Multi-partite entangled cluster states are inherently more robust than pairwise chains of entangled qubits. However, they are challenging to create as bringing together these distant nodes is often impractical. Networks of interlinked stationary (typically single atoms or ions) and flying (photonic) qubits offer a scalable route to bridging these physical distances [4], but necessitate a reliable interface between these quantum elements. A single atom strongly coupled to a single mode of the electric field, where the internal spin-state of the atom is entangled to the emitted photon polarisation, is an ideal architecture for realising such a system. The entanglement of distant atoms can then be achieved by leveraging this atom-photon entanglement. In its simplest form the transfer of a quantum state between two remote atoms can be realised by the exchange of a single-photon [5], however measurement-induced entanglement swapping actions [6, 7] on photons emitted from many atoms offer the opportunity to scale up the approach and to create arbitrary cluster states across many network nodes. Here we present the essential first step, a hybrid system where an *a priori* non-probabilistic source of polarised single-photons, produced from a single ⁸⁷Rb atom strongly coupled to an optical cavity, is used to operate a multimode interferometer (MMI) integrated onto

a photonic chip.

Coupled atom-cavity systems, with the high degree of control they provide over the light-matter interface, are a versatile tool for QIP [8–11]. Single-photon emission is one application of this interface and is *a priori* deterministic. Photons are produced in well defined quantum states, which goes beyond the intrinsically probabilistic sources, such as those based on spontaneous parametric down-conversion (SPDC), commonly used for proof-of-principle demonstrations towards linear optical quantum computing (LOQC) [12, 13]. The creation of entangled pairs of photons, emitted sequentially from a single atom [14], and of atoms, via a photon emitted by one atom and absorbed by the second [5], have been used to demonstrate atom-photon entanglement within such systems.

One can consider multiple atom-cavity systems, with distinct atomic states before and after the emission of a single-photon, each providing a different input to a multimode interferometer which implements a unitary link between inputs and outputs. In a time-resolved setting, where the time from photon emission to detection is much shorter than the photon coherence length, any detection event at an output mode projects the ensemble of input channels into an entangled cluster state. This measurement-induced entanglement relies on the unitary transformation destroying the ‘which-path’ information of the photon emission and persists until every emitted photon has been detected.

In principle any linear optics unitary operation can be realised by a series of 2×2 directional couplers [15], but such networks become increasingly complex for the creation of larger entangled states. A potentially more resource efficient and versatile tool is an MMI where every input mode is coupled to every output mode through a single waveguide. MMIs have been designed to serve a number of purposes such as demultiplexers [16, 17], power splitters [18], optical attenuators [19] and optical switches [20, 21]. By demonstrating the operation of an MMI with cavity-photons we show the ability of these in-

* now at: Bosch Car Multimedia Portugal S.A., Rua Max Grundig 35, 4705-820 Braga, Portugal

† now at: School of Physics & Astronomy, University of Nottingham, University Park, Nottingham NG7 2RD, UK

‡ now at: School of Physics and Astronomy, University of Southampton, Southampton, SO17 1BJ, UK

§ axel.kuhn@physics.ox.ac.uk

tegrated circuits to mediate the entanglement operations required for the generation of distributed cluster states in a real-world environment.

To do so we emit single-photons in well defined quantum states from a single ^{87}Rb atom coupled to a high-finesse optical cavity, and deterministically route sequential emissions down differing paths such that they are simultaneously passed through an MMI integrated onto a photonic chip. These ultra-narrow-band photons have a correspondingly long coherence time, giving rise to non-classical correlations between photon detections that are up to three orders of magnitude further apart in time than the propagation time through the chip. The quantum interference of the two photons can be contrasted to the classical behaviour observed when the input pair are made fully distinguishable, and the long temporal length of these photons allows the performance of the chip to be characterised in a time-resolved manner. We measure equivalent performance when operating the MMI to the two-photon visibility our source demonstrates in a simple Hong-Ou-Mandel (HOM) experiment. From this we conclude that our hybrid system of a cavity-based atom-photon interface and an integrated MMI is suitable for use in distributed quantum networks.

II. EXPERIMENTAL OVERVIEW

A. Single-photon generation

The photons are produced by a V-STIRAP process operating between magnetic sublevels of the ^{87}Rb D_2 line [22, 23]. The atoms are delivered stochastically into the cavity by an atomic fountain. Once there, a magnetic field lifts the degeneracy of the sublevels allowing a pump laser that is alternately tuned to either drive a Raman transition from $|F=1, m_F=+1\rangle$ to $|F=1, m_F=-1\rangle$ or visa versa, as is illustrated in figure 1(a). The second-order correlation function, $g^{(2)}(\Delta\tau)$, marked as (*) in figure 1(d) was measured using a standard Hanbury Brown-Twiss configuration [24, 25] (i.e. by detecting the photons at (*) in figure 1(b)). This shows a small, but non-negligible, $g^{(2)}(0) = 0.067$, attributable to non-Raman-resonant processes that result in the same atom emitting two photons within a driving interval. The correlation rate peaks at times corresponding to detections events an integer number of driving intervals apart. The largest peaks are measured for sequential emissions and the non-zero possibility that a spontaneous emission during photon production leaves the atom in a ‘dark’ state [26], from which it can produce no more photons, results in reduced correlation rates at longer detection time differences.

The experimental set-up required to operate the MMI chip is shown in figure 1(b), where the alternatively polarised photons are routed into paths of differing length. A 134m fibre spool delays one of the photons by the 664ns duty cycle of the production scheme such that pairs of sequentially emitted photons are delivered si-

multaneously to the MMI. Repeating a $g^{(2)}(\Delta\tau)$ measurement on the correlated detections between these two paths, shown as plot (**) in figure 1(d) and measured at (**) in figure 1(b), illustrates this routing with photon pairs only arriving in every second driving interval. The large central peaks of detections in the same time interval shows that the polarised single-photon source allows the delivery of photon pairs to be realised with increased efficiency than is possible for random routing. The smallest correlation peaks in figure 1(d)(**), corresponding to detection events an odd number of driving intervals apart, are caused by one photon taking the ‘wrong’ path, which is attributable to experimental imperfections in the polarisation state of the emitted photons, e.g. caused by a small birefringence of the cavity mirrors, and in the alignment of the polarisation-routing optical elements. These effects only result in a limited routing efficiency and so do not impact the overall two-photon interference.

The quantum interference of these photon pairs is characterised by a Hong-Ou-Mandel experiment [27, 28]. This is achieved by using a 50:50 beam splitter in place of the MMI in the configuration illustrated in figure 1(b), and rotating the relative photon polarisations at (**) to measure the orthogonally (distinguishable) and parallel (indistinguishable) polarised cases. The cross-detector correlations as a function of detection time difference at the output of this beam splitter in these two cases are compared in figure 1(e). For parallel polarised photons the suppression of these correlations illustrates the ‘bunching’ of indistinguishable pairs as they coalesce and exit into the same output mode. The two-photon visibility is defined as the reduction in likelihood of measuring cross-detector correlations for parallel polarised photons compared to the non-interfering orthogonally polarised reference. Measured over the entire interaction time of the 300ns long photons the visibility is $(70.8 \pm 4.6)\%$, which increases to $\geq 97.8\%$ when considering only detections within less than 23ns of each other. This temporal variation in the photon distinguishability is a result of their coherence properties, the theory of which is described in detail in [29]. The behaviour observed in our system indicates the interference of narrowband photons with a $2\pi \times 2.15$ MHz bandwidth. 91% of the signal arises from photon pairs of the same frequency, with the remaining contribution exhibiting a frequency difference of $\sim 2\pi \times 15$ MHz. This is the Zeeman splitting applied to the $|F=1\rangle$ ground level of our system and so suggests the presence of additional photon emission channels resulting from undesired driving processes between the magnetic sublevels. Nonetheless, within the sufficiently long coherence time the high two-photon visibility allows us to use this source to examine the interference within the MMI.

B. MMI photonic chip

The MMI on the photonic chip was fabricated using an optical lithography process to form waveguides of sil-

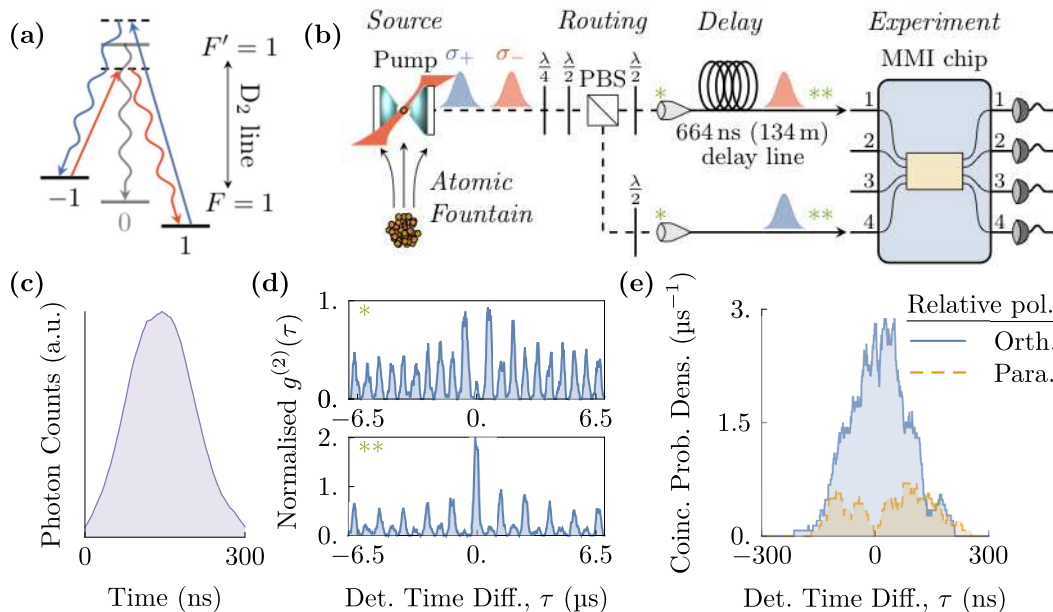


FIG. 1. (a) Energy level diagram of V-STIRAP process between magnetic sublevels of the ^{87}Rb D_2 line. (b) Experimental set-up of the hybrid source-chip system showing the routing of polarised photons into paths of different length such that pairs of photons are simultaneously delivered to the MMI chip. (c) Sliding histogram (bin width and pitch of 40 ns and 4 ns respectively) of the count rate for the 300 ns photons emitted from the source. (d) $g^{(2)}(\Delta\tau)$ measured after the Hanbury Brown-Twiss set-up both before the delay lines and with random routing of circular photons (*) and after the delay lines with deterministically routed photons (**). The plot has a bin width of 100 ns and a pitch of 20 ns. (e) Hong-Ou-Mandel interference of photon pairs on a 50:50 beam splitter, in place of the MMI chip, for parallel (indistinguishable) and orthogonally (distinguishable) polarised photon pairs, shown as a sliding histogram (bin width and pitch of 40 ns and 4 ns respectively). This gives an overall two-photon visibility of $(70.8 \pm 4.6)\%$, increasing to $\geq 97.8\%$ when considering only detections within less than 23 ns of each other.

ica doped with germanium and boron on a silicon wafer [30]. The rectangular waveguides have a $3.5\ \mu\text{m} \times 3.5\ \mu\text{m}$ cross-section and a refractive index contrast of $\Delta n = (n_{\text{core}}^2 + n_{\text{cladding}}^2) / (2n_{\text{core}}^2) \approx 0.5\%$ to support the fundamental mode at 780 nm. The four input and four output modes are all coupled to a single multimode waveguide [31] where the self-imaging principle states that the input field is then reproduced in single (or multiple) images at periodic intervals along the waveguide length [32, 33]. Coupling into and out of the chip is achieved by arrays of polarisation maintaining fibres glued directly to the chip to remove alignment mechanics.

The total loss through the chip varies from 3.3 dB to 5.9 dB across the input modes. We post-select only the experiments where the input photons are detected at the chip outputs such that the relative transmission of each input mode only affects the efficiency of data acquisition. The relevant transfer matrix, M , describing the operation of the chip is then normalised to neglect losses within the chip. This matrix was directly characterised with coherent light using the approach described in [34, 35]. Direct transmission measurements give the amplitude elements of M , with the relative offset between interference fringes measured at each output mode when driving an interferometer between pairwise combinations of input modes giving the phase information. The transfer

matrix for our MMI was measured to be

$$M = \begin{pmatrix} 0.28 & 0.7 & 0.45 & 0.48 \\ 0.41 & 0.6e^{i3.67} & 0.41e^{i3.86} & 0.54e^{i1.34} \\ 0.42 & 0.61e^{i2.84} & 0.55 & 0.38e^{i4.29} \\ 0.56 & 0.41e^{i0.39} & 0.59e^{i2.94} & 0.41e^{i4.25} \end{pmatrix}. \quad (1)$$

C. Detection-based quantum state preparation

Photon detection is performed by superconducting nanowire detectors [36] that typically measure with detection efficiencies exceeding 80%, a detection jitter of < 100 ps and recovery times of ~ 50 ns. The measured dark count rates are negligible, ranging from 5 to 66 per hour, and every detection event is recorded at run time with 81 ps precision by a commercial time-to-digital converter [37] with all data processing deferred to a later time.

The successive detections of two photons interfered through the MMI sequentially prepares then measures a cluster state of the input modes. This process can be understood by a step-by-step analysis of the system at each stage. Two indistinguishable photons input into different modes, i and j , prepares the initial state $|\Psi_{\text{in}}\rangle = \hat{a}_i^\dagger \hat{a}_j^\dagger |0\rangle$. The first detection of a photon in the output mode k –

presuming $|\Psi_{\text{in}}\rangle$ remains unchanged prior to this detection [38] – then projects the ensemble of input channels into the cluster state

$$\begin{aligned} \hat{b}_k |\Psi_{\text{in}}\rangle &= \sum_X M_{Xk} \hat{a}_k \hat{a}_i^\dagger \hat{a}_j^\dagger |0\rangle, \\ \xrightarrow{\text{norm}} \frac{M_{ik} \hat{a}_j^\dagger + M_{jk} \hat{a}_i^\dagger}{\sqrt{|M_{ik}|^2 + |M_{jk}|^2}} |0\rangle &\equiv |\Psi_{\text{cls},k}\rangle, \end{aligned} \quad (2)$$

where the action of the MMI has been described by the mappings

$$\hat{b}_i^\dagger = \sum_X M_{Xi}^* \hat{a}_X^\dagger, \quad \hat{b}_i = \sum_X M_{Xi} \hat{a}_X. \quad (3)$$

We emphasise that if the coherence length of the photons exceeds the distance between emission and detection, then any entanglement of input modes must be expressed in terms of the internal states of the emitters. Here, the spin-state of the atom, which flips upon emission, is then entangled with the photon number in the delay line. Accordingly, if multiple atom-cavity systems were used to prepare the input, the first photon detection would project the ensemble of emitters into a cluster state.

For our initial state, $|\Psi_{\text{in}}\rangle$, the probability of the first detection being in output mode k is given by

$$\begin{aligned} P_k &= \frac{\langle \Psi_{\text{in}} | \hat{b}_k^\dagger \hat{b}_k | \Psi_{\text{in}} \rangle}{\sum_X \langle \Psi_{\text{in}} | \hat{b}_X^\dagger \hat{b}_X | \Psi_{\text{in}} \rangle} = \frac{|M_{ik}|^2 + |M_{jk}|^2}{\sum_X (|M_{iX}|^2 + |M_{jX}|^2)} \\ &= \frac{1}{2} (|M_{ik}|^2 + |M_{jk}|^2) \end{aligned} \quad (4)$$

A second photon detection, in channel l , then reduces the input and output modes to the vacuum as all photons have been detected,

$$\hat{b}_l |\Psi_{\text{cls},k}\rangle = \sum_X M_{Xl} \hat{a}_X \frac{M_{ik} \hat{a}_j^\dagger + M_{jk} \hat{a}_i^\dagger}{\sqrt{|M_{ik}|^2 + |M_{jk}|^2}} |0\rangle \xrightarrow{\text{norm}} |0\rangle. \quad (5)$$

This second detection in l , conditioned on a previous detection in k , occurs with probability

$$P_{l|k} = |\langle 0 | \hat{b}_l | \Psi_{\text{cls},k} \rangle|^2 = \frac{|M_{ik} M_{jl} + M_{jk} M_{il}|^2}{2P_k}. \quad (6)$$

Repeating this analysis with the first detection in channel l followed by a second detection in k , allows us to define the probability of correlated detections between outputs k and l to be

$$\begin{aligned} Q_{ij}^{kl} &= \frac{1}{1 + \delta_{kl}} (P_k P_{l|k} + P_l P_{k|l}) \\ &= \frac{1}{1 + \delta_{kl}} |M_{ik} M_{jl} + M_{il} M_{jk}|^2, \end{aligned} \quad (7)$$

where δ_{kl} is the Kronecker delta function required to prevent double counting of the detection orders when $k = l$. For indistinguishable photons this becomes [35, 39, 40]

$$C_{ij}^{kl} = \frac{1}{1 + \delta_{kl}} (|M_{ik} M_{jl}|^2 + |M_{il} M_{jk}|^2). \quad (8)$$

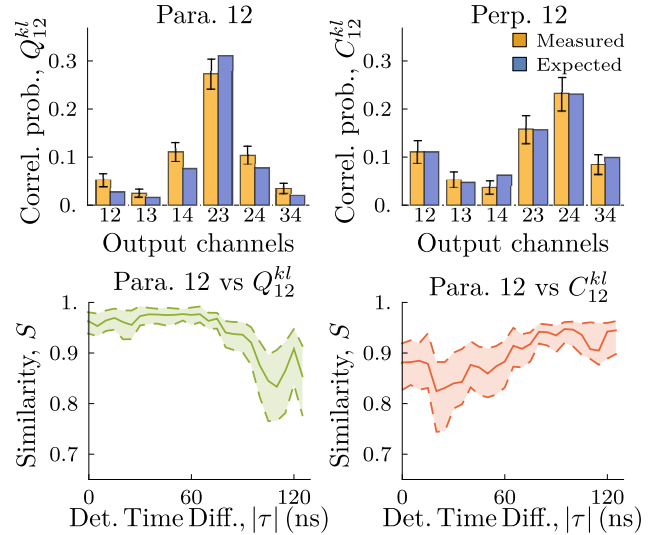


FIG. 2. Cross-detector correlations with photon pairs input into modes 1 and 2 of the MMI. The upper traces of parallel (Para. 12) and perpendicularly (Perp. 12) polarised photons show similarities to the expected behaviour of $S = 98.9_{-0.6}^{+0.4}\%$ and $S = 99.4_{-0.5}^{+0.4}\%$ respectively. The lower traces show the time-resolved performance of the parallel polarised case by comparing the measured correlation distributions to the expected behaviour for both interfering (vs Q_{12}^{kl}) and non-interfering (vs C_{12}^{kl}) photons. These consider only correlations within $|\tau| \pm 25$ ns with the dashed lines marking the 68% credible interval.

III. RESULTS

The measured distributions of cross-detector correlations for both parallel and perpendicularly polarised photon pairs input into modes 1 and 2 are shown in the upper plots of figure 2. These show similarities to the theoretically predicted distributions of $S = 98.9_{-0.6}^{+0.4}\%$ and $S = 99.4_{-0.5}^{+0.4}\%$ respectively. We follow the example of previous work [12, 30] by defining $S = \sum_i \sqrt{p_i q_i} / \sqrt{\sum_i p_i \sum_i q_i}$ where p_i and q_i are elements of the compared distributions. This is the classical fidelity normalised for distributions that do not sum to 1, as is the case here since same-detector correlations are still neglected.

Whilst identical and orthogonal distributions provide similarities of $S = 1$ and $S = 0$ respectively, pairs of randomly selected distributions do not produce similarities evenly sampled from between these bounds. For instance, the similarity between the predicted distributions for indistinguishable and fully distinguishable photon pairs in figure 2 is $S_{\text{bound}} = 90.2\%$, and two random distributions selected from within a 6-dimensional parameter space will most likely show a similarity of $87.6_{-11.6}^{+7.3}\%$ to each other [41]. That we measure parallel polarised input pairs to exhibit a similarity, to the predicted behaviour of indistinguishable two-photon states, far exceeding the expectation for classical behaviour, S_{bound} , verifies that we entangle the two input modes [42].

The long coherence length of our photons allows us to examine the performance of our hybrid source-chip system in a time-resolved manner. The lower plots of figure 2 shows the similarity of the measured correlation distribution for parallel polarised photon pairs to the predicted behaviour for both interfering (vs Q_{12}^{kl}) and non-interfering (vs C_{12}^{kl}) photons, as a function of the detection time difference. The behaviour is most similar to the interfering case, as expected, for detections up to 90 ns apart, after which the behaviour moves towards that predicted for non-interfering photons. This temporal decoherence is a property of the photons and is in agreement with that observed in their HOM interference (figure 1(e)). Photons detected 90 ns apart would correspond to a spatial separation of approximately 18 m when treating them as point particles [43], approximately 1000 longer than the chip itself, showing the two-photon state remains coherent even when the photons can naively be thought to have never been simultaneously present in the chip. The time-resolved similarity of the measured data to the expected behaviour for interfering photons never exceeds the equivalent similarity quoted when considering all correlations. This is because these smaller data sets are also more susceptible to statistical noise, which is more likely to negatively impact the similarity than positively.

To fully characterise the performance of the MMI the same-detector correlations, many of which are missed due to the finite recovery time of the detectors, must be considered. The distribution of all correlations, both same- and cross-detector, is given by the autoconvolution of the intensity profile of the photons (seen in figure 1(c)). By matching this profile to the measured distribution of correlations separated by more than the maximum detector recovery time, τ_R , we can infer the number of missed correlations as can be seen in the upper left plot of figure 3.

To find how these missed same-detector correlations should be distributed across the output channels, we note from equations (7) and (8) that $Q_{ij}^{kk}/C_{ij}^{kk} = 2$. As this relationship holds for any choice of input and output modes, the relative distribution of these same-detector correlations is unchanged by the photon distinguishability. Thus for a given data set we can find this relative distribution by considering correlations between photons made fully distinguishable in time. The upper right plot of figure 3 shows these when considering detection time differences of twice the duty cycle of the experiment, corresponding to the nearest side-peaks to the central peak for the $g^{(2)}$ ($\Delta\tau$) measured with photon routing and delay lines in place in figure 1(d). Physically these are events where the production of the second photon succeeds on the second attempt at producing that polarisation and so effectively there are two duty cycles between detections. As this is much longer than the detector recovery times, no same-detector correlations are missed in this case.

The lower traces in figure 3 show the complete corrected performance of the MMI for both parallel and perpendicularly polarised photons input into modes 1 and

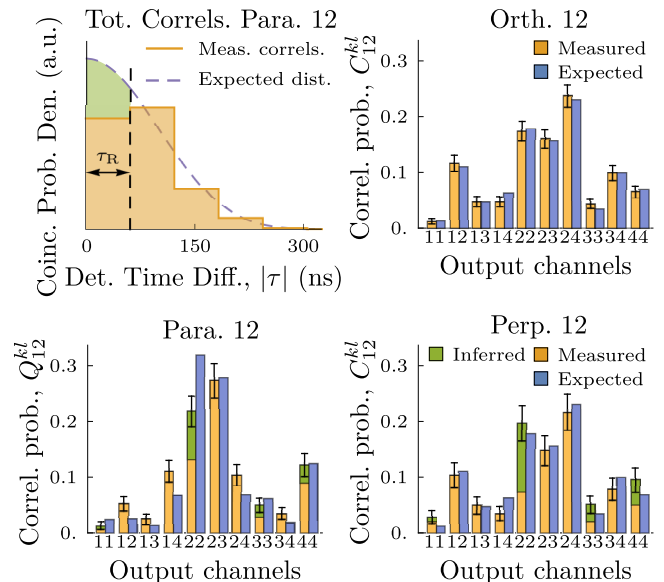


FIG. 3. Performance of the chip for photon pairs input into modes 1 and 2, corrected for missing same-detector correlations due to the finite recovery time, τ_R . The upper left plot compares the distribution of all measured correlations to that expected – found as described in the text – from which the total number of missed detections can be inferred. The distribution of these is known to be the same regardless of the photon interference, and so can be found by looking at the same-detector correlations observed for orthogonal photons (Orth. 12 with $S = 99.6^{+0.2}_{-0.2}\%$) – ‘orthogonal’ here referring to the property of the photon states not overlapping in time. Their polarisation is then not relevant, and indeed is parallel for the data shown here. The lower traces show the complete data, including this same-detector correction, for both parallel (Para. 12, $S = 98.3^{+0.5}_{-0.6}\%$) and perpendicularly (Perp. 12, $S = 98.9^{+0.5}_{-0.5}\%$) polarised input photons.

2 measured across all possible output pairings. These have similarities (or equivalently fidelities as our distributions now sum to one) to the theoretical predictions of $S = 98.3^{+0.5}_{-0.6}\%$ and $S = 98.9^{+0.5}_{-0.5}\%$ respectively.

The chip operation with photons input to modes 1 and 3 is summarised in figure 4 where the parallel polarised photons show $S = 97.7^{+0.6}_{-0.6}\%$ to the predicted behaviour. Orthogonal input photons, made distinguishable in time, show $S = 99.4^{+0.3}_{-0.4}\%$.

The performance of our hybrid chip-source system clearly indicates the successful operation of the MMI with cavity-photons. To quantify whether the rather small imperfections arise from the observed photon decoherence we can consider that for an input pair with two-photon visibility, V , the expected output is simply the weighted average of the limiting cases,

$$R_{ij}^{kl}(V) = V \cdot Q_{ij}^{kl} + (1 - V) \cdot C_{ij}^{kl}, \quad (9)$$

where $0 \leq V \leq 1$, with $V = 0$ ($V = 1$) corresponding to completely distinguishable (indistinguishable) photons.

The distributions $R_{12}^{kl}(V_{12})$ and $R_{13}^{kl}(V_{13})$ show maximum similarities to the observed behaviour of parallel

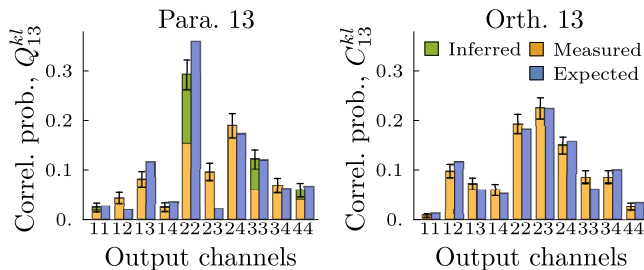


FIG. 4. Performance of the chip measured for photon pairs input into modes 1 and 3, including a correction for the inferred missed same-detector correlations. The distribution of correlations separated by less than the photon length for parallel polarised input photons (Para. 13) shows a similarity to the expected behaviour of $S = 97.7_{-0.6}^{+0.8}\%$. Orthogonal input photons made distinguishable in time (Orth. 13) taken from the same experimental run show $S = 99.4_{-0.4}^{+0.3}\%$.

polarised photons input to modes 1 and 2 (see figure 3) and modes 1 and 3 (see figure 4) of $S = 99.1_{-0.3}^{+0.3}\%$ and $S = 99.4_{-0.3}^{+0.2}\%$ respectively for $V_{12} = 0.728$ and $V_{13} = 0.684$. This is in good agreement with the two-photon visibility of $(70.8 \pm 4.6)\%$ observed from the HOM interference of our photons, from which we can conclude that the performance of our system is not impacted by any additional decoherence arising from the interfacing of the atom-cavity source with the photonic MMI chip.

IV. CONCLUSIONS

Having found similarities with the expected quantum behaviour in the MMI output exceeding 95% for correlations several tens of ns apart impressively show the potential of our hybrid approach. First, they clearly demonstrate quantum supremacy in the multimode interferometry of cavity photons. Second, the long time span between detections demonstrates that the MMI effectively projects the entire input vector into an entangled cluster state upon the first detection, which survives and preserves its coherence until the second photon is detected. To this respect, the similarity recorded as a function of detection-time difference can be regarded as the fidelity of remaining in the cluster state probabilistically prepared upon the first photon detection.

While our present study demonstrates the feasibility of cluster-state preparation, this actually happens between the atom-cavity system, and the photon state stored in an optical fibre. For future quantum networking, we anticipate the implementation of a network of atom-cavity systems, all coupled simultaneously by fibres to a photonic MMI chip. First detections in the MMI output will then project the ensemble of input atoms into a spatially distributed cluster state. To allow entanglement to persist after all photons are detected, the atom-cavity system must entangle the internal spin-state of the atom with the emitted photon polarisation, requiring a polarised scheme such as ours. Different measurement outcomes that depend on the distinguishability, and hence interference through the unitary, of the input multi-photon state can then probabilistically project the atoms into an entangled state.

In summary the combination of our single-photon source with an integrated photonic chip, each of which was individually characterised, has been shown to operate without any measurable flaws arising from their unification and in full accordance with expectations. This is an important step towards a distributed quantum network of cavity-based emitter-photon entanglers as it proves the ability, in a real-world setting, of integrated MMIs to mediate multi-partite entanglement across numerous distant nodes in a quantum network. This is also the first time an atom-cavity single-photon source that provides polarisation control has been integrated with a more complex optical network than a simple beam-splitter. This control could be combined with readily available fast-switching electro-optical elements such as Pockels cells to allow active routing of the photons, and thus the non-probabilistic preparation of larger Fock states [44, 45]. This is a promising approach to surpassing the random photon routing that has limited the photon number of equivalent experiments with previous cavity-based [12] and SPDC sources [31, 40, 46].

ACKNOWLEDGMENTS

We acknowledge support for this work through the quantum technologies programme (NQIT hub). The authors are also grateful to Chris Sparrow for his helpful discussions.

-
- [1] R. Raussendorf, D. E. Browne, and H. J. Briegel, *Physical review A* **68**, 022312 (2003).
 - [2] M. A. Nielsen, *Rep. Math. Phys* **57**, 147 (2006).
 - [3] R. Jozsa, *NATO Science Series, III: Computer and Systems Sciences. Quantum Information Processing-From Theory to Experiment* **199**, 137 (2006).
 - [4] A. Reiserer and G. Rempe, *Reviews of Modern Physics* **87**, 1379 (2015).
 - [5] S. Ritter, C. Nolleke, C. Hahn, A. Reiserer, A. Neuzner,

- M. Uphoff, M. Mücke, E. Figueroa, J. Bochmann, and G. Rempe, *Nature* **484**, 195 (2012).
- [6] D. Moehring, P. Maunz, S. Olmschenk, K. Younge, D. Matsukevich, L.-M. Duan, and C. Monroe, *Nature* **449**, 68 (2007).
- [7] S. Olmschenk, D. Matsukevich, P. Maunz, D. Hayes, L.-M. Duan, and C. Monroe, *Science* **323**, 486 (2009).
- [8] A. Kuhn, M. Hennrich, and G. Rempe, *Phys. Rev. Lett.* **89**, 067901 (2002).

- [9] G. S. Vasilev, D. Ljunggren, and A. Kuhn, *New Journal of Physics* **12**, 063024 (2010).
- [10] J. Dilley, P. Nisbet-Jones, B. W. Shore, and A. Kuhn, *Physical Review A* **85**, 023834 (2012).
- [11] P. B. R. Nisbet-Jones, J. Dilley, A. Holleczek, O. Barter, and A. Kuhn, *New Journal of Physics* **15**, 053007 (2013).
- [12] A. Holleczek, O. Barter, A. Rubenok, J. Dilley, P. B. R. Nisbet-Jones, G. Langfahl-Klabes, G. D. Marshall, C. Sparrow, J. L. O'Brien, K. Poulios, A. Kuhn, and J. C. F. Matthews, *Phys. Rev. Lett.* **117**, 023602 (2016).
- [13] O. Barter, *Deterministic Quantum Feedback Control in Probabilistic Atom-Photon Entanglement*, Ph.D. thesis, University of Oxford (2016).
- [14] T. Wilk, S. C. Webster, A. Kuhn, and G. Rempe, *Science* **317**, 488 (2007).
- [15] M. Reck, A. Zeilinger, H. J. Bernstein, and P. Bertani, *Phys. Rev. Lett.* **73**, 58 (1994).
- [16] J.-K. Hong and S.-S. Lee, *J. Lightwave Technol.* **25**, 1264 (2007).
- [17] J. Xiao, X. Liu, and X. Sun, *Opt. Express* **15**, 8300 (2007).
- [18] D. J. Y. Feng and T. S. Lay, *Opt. Express* **16**, 7175 (2008).
- [19] X. Jiang, X. Li, H. Zhou, J. Yang, M. Wang, Y. Wu, and S. Ishikawa, *IEEE Photonics Technology Letters* **17**, 2361 (2005).
- [20] S. Nagai, G. Morishima, H. Inayoshi, and K. Utaka, *Journal of Lightwave Technology* **20**, 675 (2002).
- [21] F. Wang, J. Yang, L. Chen, X. Jiang, and M. Wang, *IEEE Photonics Technology Letters* **18**, 421 (2006).
- [22] T. Wilk, H. P. Specht, S. C. Webster, G. Rempe, and A. Kuhn, *Journal of Modern Optics* **54**, 1569 (2007).
- [23] T. Wilk, S. C. Webster, H. P. Specht, G. Rempe, and A. Kuhn, *Phys. Rev. Lett.* **98**, 063601 (2007).
- [24] R. Hanbury Brown and R. Q. Twiss, *Nature* **177**, 27 EP (1956).
- [25] R. Hanbury Brown and R. Q. Twiss, *Nature* **178**, 1046 EP (1956).
- [26] T. D. Barrett *et al.*, arXiv:1804.10455 (2018).
- [27] C. K. Hong, Z. Y. Ou, and L. Mandel, *Phys. Rev. Lett.* **59**, 2044 (1987).
- [28] T. Legero, T. Wilk, M. Hennrich, G. Rempe, and A. Kuhn, *Phys. Rev. Lett.* **93**, 070503 (2004).
- [29] T. Legero, T. Wilk, A. Kuhn, and G. Rempe, *Advances In Atomic, Molecular, and Optical Physics* **53**, 253 (2006).
- [30] A. Politi, M. J. Cryan, J. G. Rarity, S. Yu, and J. L. O'Brien, *Science* **320**, 646 (2008).
- [31] A. Peruzzo, A. Laing, A. Politi, T. Rudolph, and J. L. O'Brien, *Nature Communications* **2**, 224 (2011).
- [32] R. Ulrich, *Optics Communications* **13**, 259 (1975).
- [33] R. Ulrich, *Nouvelle Revue d'Optique* **6**, 253 (1975).
- [34] S. Rahimi-Keshari, A. Scherer, A. Mann, A. T. Rezakhani, A. I. Lvovsky, and B. C. Sanders, *New Journal of Physics* **13**, 013006 (2011).
- [35] S. Rahimi-Keshari, M. A. Broome, R. Fickler, A. Fedrizzi, T. C. Ralph, and A. G. White, *Opt. Express* **21**, 13450 (2013).
- [36] Photon Spot, model number NW1FC780.
- [37] Qutools quTAU.
- [38] When measuring a superposition of multi-photon Fock states with wavepacket lengths exceeding the detector time resolution, the absence of a photon detection in some time interval would provide information on the nature of the state resulting in a time-dependent evolution. The possibility of a two-photon state in an output mode of the MMI might lead to a time-dependence in the cluster states prepared by the first detection, however this does not affect the overall probability for correlations and a full treatment of this effect is beyond the scope of this paper.
- [39] K. Mattle, M. Michler, H. Weinfurter, A. Zeilinger, and M. Zukowski, *Applied Physics B: Lasers and Optics*, **60**, S111 (1995).
- [40] K. Poulios, R. Keil, D. Fry, J. D. A. Meinecke, J. C. F. Matthews, A. Politi, M. Lobino, M. Gräfe, M. Heinrich, S. Nolte, A. Szameit, and J. L. O'Brien, *Phys. Rev. Lett.* **112**, 143604 (2014).
- [41] The asymmetric error bars on quoted similarities denote the 68% credible interval, given by the corresponding highest posterior density interval. The distribution of possible similarities from which these are derived is found using Monte Carlo methods.
- [42] B. M. Terhal and P. Horodecki, *Phys. Rev. A* **61**, 040301 (2000).
- [43] Using the reasonable approximation that the speed of light in a fibre is $2c/3$.
- [44] H. Wang, Y. He, Y.-H. Li, Z.-E. Su, B. Li, H.-L. Huang, X. Ding, M.-C. Chen, C. Liu, J. Qin, *et al.*, *Nature Photonics* **11**, 361 (2017).
- [45] T. Pittman, B. Jacobs, and J. Franson, *Physical Review A* **66**, 042303 (2002).
- [46] K. Poulios, D. Fry, A. Politi, N. Ismail, K. Wörhoff, J. L. O'Brien, and M. G. Thompson, *Opt. Express* **21**, 23401 (2013).